2019

Evaluation of additively manufactured microchannel heat sinks

I. L. Collins
Purdue University

J. A. Weibel
Purdue University, jaweibel@purdue.edu

L. Pan
Purdue University

S V. Garimella
Purdue University, sureshg@purdue.edu

Collins, I. L.; Weibel, J. A.; Pan, L.; and Garimella, S V., "Evaluation of additively manufactured microchannel heat sinks" (2019). *CTRC Research Publications*. Paper 349.
http://dx.doi.org/10.1109/TCPMT.2018.2866972

Evaluation of Additively Manufactured Microchannel Heat Sinks

Ivel L. Collins, Justin A. Weibel, Liang Pan, Suresh V. Garimella

***Abstract*— Microchannel heat sinks allow removal of dense heat loads from high-power electronic devices at modest chip temperature rises. Such heat sinks are produced primarily using conventional subtractive machining techniques or anisotropic chemical etching, which restricts the geometric features that can be produced. Owing to their layer-by-layer and direct-write approaches, additive manufacturing (AM) technologies enable more design-driven construction flexibility and offer improved geometric freedom. Various AM processes and materials are available, but their capability to produce features desirable for microchannel heat sinks has received limited assessment. Following a survey of commercially mature AM techniques, direct metal laser sintering (DMLS) was used in this work to produce both straight and manifold microchannel designs with hydraulic diameters of 500 μm in an aluminum alloy (AlSi10Mg). Thermal and hydraulic performance were characterized over a range of mass fluxes from 500 kg/m²s to 2000 kg/m²s using water as the working fluid. The straight microchannel design allows these experimental results to be directly compared against widely accepted correlations from the literature. The manifold design demonstrates a more complex geometry that offers a reduced pressure drop. A comparison of the measured and predicted performance confirms that the nominal geometry is reproduced accurately enough to predict pressure drop based on conventional hydrodynamic theory, albeit with roughness-induced early transition to turbulence; however, the material properties are not known with sufficient accuracy to allow for *a priori* thermal design. New design guidelines are needed to exploit the benefits of additive manufacturing while avoiding undesired or unanticipated performance impacts.**

***Index Terms*—additive manufacturing, direct metal laser sintering, microchannel heat sink, microchannel heat exchanger, power electronics**

NOMENCLATURE

A_{ch}	channel cross-sectional area
D_H	hydraulic diameter
f_F	Fanning friction factor
f_1, f_2	friction coefficients in Eq. (7) and (8)
G	mass flux
K_∞	Hagenbach factor
L_{ch}	channel length
L_{dev}	developing flow length
h	heat transfer coefficient
Nu	Nusselt number
P	perimeter
Pr	Prandtl number
Q_{in}	heat input
R	thermal resistance
Re	Reynolds number
T	temperature
$\dot{V}$	volumetric flow rate
ΔP	pressure drop
Greek Symbols	
α	aspect ratio
μ	dynamic viscosity
η	efficiency
ρ	density
Subscripts	
amb	ambient
avg	arithmetic mean
$base$	heat sink base
cal	caloric
$cond$	conductive
$conv$	convective
fd	fully developed
fin	individual fin
in	evaluated at the heat sink inlet
l	liquid
o	overall surface efficiency
out	evaluated at the heat sink outlet
s	evaluated for the solid material
tot	total
$wall$	average over the channel wall

I. INTRODUCTION

THE need for compact packaging of high-power electronics has challenged the capacity of forced air convection as a cooling approach, necessitating a shift toward microscale liquid cooling techniques in order to provide the required heat dissipation. Microchannel heat sinks are of significant technological interest; a variety of channel sizes, cross-sectional shapes, and fluids have been studied under both single- and two-phase flow conditions [1], [2]. Microchannel heat sink geometries have typically been numerically optimized for single-phase flow conditions [3]–[5].

One drawback of microchannels is the high pressure drop associated with flow through the heat sink, which can be

Manuscript submitted on 20 March, 2018. This work was supported by the Cooling Technologies Research Center, a graduated National Science Foundation Industry/University Cooperative Research Center at Purdue University.

The authors are with the Cooling Technologies Research Center and the School of Mechanical Engineering, Purdue University, West Lafayette, IN 47907-2088 USA (e-mail: ivellee.collins@gmail.com, jaweibel@purdue.edu, liangpan@purdue.edu, sureshg@purdue.edu).

alleviated by the addition of a manifold layer [6]. Such manifold microchannel (MMC) heat sinks reduce pressure drop by decreasing the flow length within the microchannels. Shorter flow lengths also result in a greater portion of the heat sink area experiencing higher heat transfer coefficients associated with developing boundary layers. Manifold designs allow for greater control over surface temperature uniformity and can lead to lower thermal resistances at a fixed pumping power than conventional designs [7]. Manifold microchannel heat sink designs have been optimized for various performance objectives [8], [9] and dissipation of heat fluxes above 1 kW/cm^2 has been experimentally demonstrated [10], [11].

Microchannel heat sinks have been typically produced using traditional subtractive machining (*e.g.*, dicing, micro-milling) or microfabrication approaches (*e.g.*, deep reactive ion etching, LIGA). The channels are often produced on a silicon substrate to mimic direct embedding in a computer chip, or on metal substrates in the case of attached heat sinks and heat exchanger applications. These fabrication approaches suffer from geometric restrictions; features must be generally rectangular and exist in a single plane. Complex design features such as three-dimensional curves or channels are exceedingly difficult or impossible to fabricate. Heat sinks also require attachment of a secondary lid to seal the channels; in the case of MMC designs, bonding of several layers including the manifold may become necessary.

A new additive manufacturing paradigm evolved from the pioneering work of Kodama in the early 1980s, who developed a technique to fabricate 3D structures by selectively curing layers of a photosensitive resin with a UV light source [12]. This technique was quickly commercialized and is now commonly known as stereolithography (SLA). Additional techniques including fused deposition modeling (FDM) and laminated object manufacturing (LOM) were developed and commercialized by the early 1990s [13]. Selective laser sintering (SLS), a process that uses a directed energy source (*e.g.*, laser) to fuse powdered material, was developed by Deckard in 1989 [14]. Laser sintering technology was a crucial step forward that enabled the use of metal powders to produce components. Despite significant refinement of the fabrication processes and introduction of new materials throughout the next two decades, additive manufacturing remained largely confined to prototyping and research applications.

In recent years, additively manufactured parts have begun to appear in aerospace applications, where potential weight reduction and geometric flexibility are worth the cost associated with producing and qualifying the parts. Many companies, such as GE Aviation and Airbus, have leveraged additive manufacturing systems to produce parts such as fuel nozzles, brackets, hinges, and tooling [15]. The National Aeronautics and Space Administration (NASA) has invested heavily in additive technologies and has produced different engine components including combustion chambers, turbines, pump housings, and injectors [16], [17]. While these efforts illustrate the value of AM to industry, they also highlight challenges facing widespread commercial usage, including accurate prediction of material properties, part repeatability, process standardization, and effective quality control [18].

To date there has been little work focused on additively manufactured microchannel heat sinks and heat exchangers, with even fewer studies targeted specifically at electronics thermal management applications. A number of studies have explored the manufacture of small channels using powder bed fusion additive processes. Stimpson *et al.* [19], [20] characterized the effects of surface roughness on microchannel performance for gas turbine cooling applications, finding that parts produced with direct metal laser sintering (DMLS) have significantly higher roughness than machined components; this roughness significantly affects the hydraulic and thermal performance of the channels. Snyder *et al.* [21] also found that channel roughness significantly affected friction factor, but not Nusselt number.

Kirsch and Thole [22] compared additively (Inconel 718; DMLS) and conventionally manufactured pin fin heat exchangers having arrays of small cylindrical fins within a 25.4 × 25.4 × 1 mm^3 duct. Due to high internal surface roughness, the additively manufactured arrays demonstrated significantly higher (20-60%) friction factors than comparable smooth pin fin arrays; the Nusselt number augmentation was marginal and was more significant at tighter spacings. Kirsch *et al.* [23] demonstrated that fabrication of identical nominal geometries using different materials resulted in large variations in the actual geometry of the part produced. Changing a single machine parameter can have an outsized impact on performance; for example, changing the beam offset by a small amount led to a three-times increase in friction factor.

Arie *et al.* [24] numerically optimized air-liquid heat exchangers based on the state-of-the-art fabrication process limitations of DMLS and demonstrated that designs tailored to the capabilities of additive manufacturing can result in significant performance improvements compared to many conventional heat exchange surfaces. A manifold air-water heat exchanger was produced using DMLS in titanium [25] based on the design optimization. Despite geometric inconsistencies between the design and the printed part, the heat exchanger demonstrated 15-50% higher heat transfer coefficients at a constant pressure drop compared to other types of commonly used heat exchanger surfaces.

Other work on additively manufactured heat exchangers includes the fabrication of a polymer-metal composite heat exchanger using fused deposition techniques as a low-cost alternative for dry cooling towers [26]. Dede *et al.* [27] fabricated an optimized aluminum alloy heat sink design using additive manufacturing for jet impingement air cooling, which achieved performance superior to various standard designs. Wong *et al.* [28] demonstrated the value of additive manufacturing with a variety of pin-fin geometries designed to improve heat transfer performance through surface area augmentation. They noted that developing higher-conductivity alloys, improving part density, and enhancing surface finish were challenges that needed to be addressed to fully utilize the potential of the technology. Gerstler and Erno [29] additively manufactured an Inconel heat exchanger (oil cooler) for airborne turbine engines; the DMLS-produced design was lighter, smaller, operated closer to specified pressure drop limits, and had a slight improvement in heat transfer performance compared to the existing design. Scheithauer *et al.* [30] produced a ceramic heat exchanger with a complex three-dimensional geometry that could only be fabricated with

additive manufacturing; they identified key challenges with respect to the optimization of additive designs.

As the range of viable commercial applications of additive manufacturing technology continues to expand, it stands to offer large benefits to the heat exchange industry whose products rely on complex geometry to enhance performance and efficiency. However, as the limited research into this area has found, the processes underlying additive manufacturing must be evaluated and understood before it can be fully utilized. Many technologies do not accurately reproduce the heat sink geometry, and the properties resulting from the manufacturing process lead to concerns such as surface roughness that must be quantified and taken into account when designing for additive production. Nearly all of the additively produced thermal management components presented above use a variation of a powder bed fusion process (DMLS); the justification for this choice is not discussed in the associated publications.

The current work surveys AM technologies to determine the techniques that are likely capable of producing desirable heat sink features and to explain the selection criteria for a microchannel heat sink application. After identification of feasible processes and consideration of their capabilities relative to this application, DMLS is utilized to produce several heat sink designs. The heat sinks are experimentally characterized to assess their performance relative to design predictions, as well as to demonstrate how the AM technology can readily produce features that offer a performance benefit. Discrepancies between the measured and predicted performance, owing to characteristics of the additive manufacturing process, are discussed.

II. Process Selection

Desirable features that beneficially manipulate flow in microchannel heat sinks include convective enhancements, channels with variable cross-sections, and fully three-dimensional flow paths (including out-of-plane directions). Fabrication approaches must offer the ability to design for high-heat-flux, low-thermal-resistance operation and hotspot targeting, potentially via integrated manifolds. The surface finish, geometric accuracy, and the ability to produce the heat sink as a single monolithic piece are also of concern. Materials used for heat sinks must typically offer high conductivity, low weight, and compatibility with the variety of liquids that are commonly used in applications, including water, refrigerants, and dielectrics. Two-phase operation would require the consideration of additional features such as nucleation site enhancements and vapor extraction, but is not the focus of the current study.

Many of these heat sink features have overlapping fabrication requirements that map to a short list of desirable additive manufacturing process capabilities. Small feature sizes would allow for channel-level convective enhancements and controlled channel geometry. Consideration of the desired design capabilities requires additive processes capable of producing complex internal geometries such as perpendicular unsupported surfaces, thin walls, and flexibility in build orientation. The materials selection should offer high thermal conductivity and low porosity. Material choice, surface orientation, and process parameters (*e.g.*, laser power, scan speed) all influence surface finish [19], [20], [31].

Current state-of-the-art process capabilities of additive manufacturing techniques were surveyed to identify those most suitable for microchannel heat sink applications. The survey was restricted to commercially available, mature techniques that have product literature available. Information on process capabilities and specifications was obtained from additive manufacturing equipment vendors, services, and academic reviews [32]–[35]. For specifications such as the minimum feature size, the manufacturer-quoted machine capabilities often did not align with services offered by third-party vendors. A representative range of values can be estimated by comparing multiple pieces of equipment using the same technique. Due to the rapid pace of research advances into nearly all additive manufacturing techniques, it is expected that processes, equipment, and materials selection will improve and expand the design space available. The conclusions of this survey extend to other thermal management applications that share similar feature requirements, such as for compact heat exchangers.

After compiling information on a wide variety of AM technologies, they were assessed for application feasibility. Materials requirements restrict selection to processes capable of utilizing metals, eliminating widely used techniques such as SLA and FDM. The desire for complex internal geometries further eliminates directed energy deposition methods such as laser engineered net shaping (LENS) [36], which use a powder or wire feed and an energy source to deposit molten metal where desired. These processes generally have larger minimum feature sizes and lower resolution than would be preferred for this application. Binder jetting, a technique that first utilizes a resin to bind particles together into a ‘green’ part which is then sintered to produce the final solid piece, is another option. Binder jetting has advantages in materials selection, build speed, and total build volume; however, shrinkage during sintering and difficulty in producing fully dense parts [37] are significant concerns for the production of microchannel heat sinks.

The remaining AM techniques considered include powder bed fusion processes and electrochemical fabrication. For powder bed fusion processes, a laser or an electron beam is typically used as the energy source; these are respectively referred to as direct metal laser sintering (DMLS) and electron beam melting (EBM) in the text to follow. Electrochemical fabrication (EFAB) refers to a class of processes utilizing conventional photolithography and electrodeposition of metals. This layer-by-layer technique electrodeposits metal on top of a photo-defined sacrificial support layer, filling the cross-section where solid geometry is needed. Each layer is planarized and the support structure is chemically etched away after all layers are formed, leaving behind a solid metal structure.

Table I shows a comparison of the typical process capabilities for DMLS, EBM, and EFAB. Because DMLS and EBM differ only in terms of the energy source, the capabilities and materials available for each are largely identical; minimum feature sizes of approximately 200-400 μm with 50 μm tolerances are possible, and a range of tool and stainless steels,

nickel-based alloys, titanium, and aluminum can be used. Laser-based systems are available from a number of manufacturers (*e.g.*, EOS, Renishaw, Concept Laser) and are widely used; electron beam systems are rarer (produced by Arcam Ab). Electrochemical fabrication processes have a clear advantage with respect to feature size and can produce features under 25 µm with 2 µm tolerances, but support a more limited range of materials and have small build volumes. Additionally, EFAB processes have fewer commercial vendors (*e.g.*, Microfabrica MICA Freeform); similar technology appears to have been developed for internal use at other companies (*e.g.*, Rockwell Collins Z-fab). Based on these considerations, DMLS was selected as the AM technique to fabricate the microchannel heat sinks for the present work as detailed in the following section.

III. Experimental Methods

A. Heat Sink Design and Fabrication

A conventional straight-channel design is first investigated in order to demonstrate the additive manufacturing and testing of a microchannel heat sink. This design allows comparison of the experimental results to well-established correlations to determine if any discrepancies in performance can be attributed to the manufacturing technique. The geometric simplicity also reduces challenges associated with producing small interior geometry with a powder bed fusion process in this baseline step. The geometry selected for this heat sink is based on conservative fabrication constraints rather than optimized performance.

The straight microchannel (SMC) design (Fig. 1a) consists of sixteen identical channels of square cross section running lengthwise along the heat sink and covering a 15 mm × 15.5 mm footprint area. The channels share common inlet and outlet headers, with pressure taps located at each end of the channel. The critical dimensions of the heat sink geometry were chosen primarily based on the surveyed capabilities of the selected DMLS process, namely, a minimum feature size of ~150 µm and minimum solid wall thickness of ~300 µm, with ~50 µm tolerances. The square channel size was conservatively chosen to be 500 µm × 500 µm (D_H = 500 µm), an order of magnitude larger than the nominal tolerance. The solid walls between the channels also have a cross-section of 500 µm × 500 µm and act as fins to increase the heat transfer area. The solid base thickness is 1 mm to reduce the potential for leakage due to porosity of the material, with a 250 µm-deep, 1000 µm-wide groove running from one edge of the base surface to the center to allow placement of a thermocouple to measure the temperature at the center of the base.

Though useful for comparing the results to conventional correlations, straight microchannels do not demonstrate the value added by AM in terms of geometric featuring. A second manifold microchannel (MMC) design (Fig. 1b) was investigated in order to demonstrate additive manufacturing of a more complex heat sink geometry that offers potential performance benefits. A top manifold layer is incorporated to split the flow in parallel into multiple inlets and outlets along any one microchannel. This reduces the maximum flow length through the microchannel cross-section, thereby decreasing the pressure drop along the heat sink. The bottom layer of microchannels retains the same dimensions as in the straight microchannel design; the base thickness is the same. The manifold layer is 1.50 mm thick with 1.00 mm-wide walls separating the manifold inlets and outlets. Several studies have shown that for single-phase flow the optimal ratio between the manifold inlet width and the manifold outlet width is 3:1 [8], [9]. A 1.50 mm-wide inlet and 0.50 mm-wide outlet are chosen accordingly, leading to an effective flow length of 2.00 mm through the microchannels, compared to the 15.00 mm flow length of the straight microchannel design.

Though it is possible to fabricate both of these designs using conventional manufacturing processes, additive manufacturing offers the advantage of monolithic construction. Subtractive cutting/etching of straight microchannels into a substrate requires that a separate lid be sealed on top of the heat sink; the manifold design requires three layers (microchannels, manifold, and lid) to be aligned and sealed. In comparison, the heat sinks are produced herein as a single part without requiring any assembly.

Both heat sink designs were fabricated using DMLS (EOS M280) through a commercial vendor (GPI Prototype & Manufacturing Services); the material is AlSi10Mg. Aside from removal of the support substrate using wire electric discharge machining, no post-machining or post-treatment processes were applied to the part after fabrication. Interferometry measurements (Zygo, NewView 6200) of the exterior surfaces showed that the surface roughness (Ra) is ~ 20 µm, double the nominal manufacturer-specified value [38] and similar to that of other additively produced aluminum pieces [28]. The exterior surface roughness is visible in Fig. 2, which shows photographs of the two heat sinks, with cutouts to allow for visual inspection, produced using the same process and equipment as the samples fabricated for experimental characterization. The surface roughness on the interior features is qualitatively higher due to 'burn', *i.e.*, partial sintering of loose powder to nearby solid features that can be exacerbated by heat build-up within the part during fabrication. Micro-computed tomography (µCT) scanning was used to non-destructively investigate the porosity of the material produced using this DMLS process. A small (1.5 mm × 1.5 mm × 1.5 mm) cube of the material was fabricated for the purpose and scanned (Bruker microCT, SkyScan 1172); the porosity was <0.1%, within the stated range for the material [38]. This sample cube was fabricated using the same processing parameters as the heat sinks and is therefore representative of the solid printed material in the heat sinks.

B. Experimental Facility

A flow loop facility (Fig. 3) was constructed to characterize the hydraulic and thermal performance of the additively manufactured microchannel heat sinks. The working fluid, deionized water, is circulated through the closed loop at a constant flow rate using a gear pump (Micropump, DP-415A drive with a GA-T23 pump); this positive displacement pump ensures that the same range of flow rates can be tested regardless of changes in the pressure drop between heat sink designs. A 7 µm particulate filter is used to remove debris from

the fluid and is sized to be smaller than the diameter range of the powder particles used to produce the heat sinks (~ 30-70 μm) in the event that loosely sintered particles become dislodged during operation. The flow rate is measured using a turbine-style flow meter (McMillan, 106-5DHT, 50-500 mL/min, ±1.0% FS) and then preheated to set a constant temperature at the inlet of the test section using a heating cable wound around the stainless steel tubing and a temperature controller (Glas-Col, TOT-1200). For all tests, the temperature of the fluid at the inlet of the test section is 30 °C. After passing through the test section, the flow is cooled by passing through a custom tube-in-tube heat exchanger before being returned to the reservoir. Cooling water flows through a secondary loop; this is not shown in the figure. The reservoir is sealed, but flexible, such that the reservoir pressure is maintained equal to the ambient pressure during testing. It is important to note that in many applications the material compatibility of aluminum alloys and deionized water may be of concern for long-term operation. Compatibility was not evaluated in the present work, and was not relevant for the short duration of the experiments conducted.

Within the test section (Fig. 4), two T-type thermocouples (Omega, TJ36-CPSS-020U-6, ±1.0 °C) measure the inlet and outlet temperature of the water entering the heat sink; a third T-type thermocouple (Omega, 5TC-TT-T-40-36, ±1.0 °C) measures the heat sink base temperature from within the groove on the base heat sink surface. The differential pressure is measured (Omega, PX2300-10DI, 0-10 psi, ±0.25% FS) across the microchannels using the inlet and outlet pressure taps within the heat sink. The positioning of the pressure taps immediately upstream and downstream of the microchannels avoids the minor losses in the inlet and outlet headers being included in this measurement. Prior to assembling the test section, the top and bottom surfaces of the heat sink are manually polished with 1000-grit sandpaper in order to allow for a better seal against o-rings on the top surface and better contact with the heater on the bottom. Power to the heat sink base is provided by a 12 × 12 mm^2 ceramic heater (Ultramic, CER-1-01-00334, 200 W). Voltage is measured across the heater; current is measured using a shunt resistor. A thermal gap pad (Bergquist, Gap Pad A3000) is placed between the heater and the heat sink surface to limit the temperature rise of the heater and provide a consistent thermal interface resistance for purposes of calibrating the heat loss. A polyether ether ketone (PEEK) spacer helps position the heater with respect to the heat sink and insulates the backside of the heater to minimize heat losses. After assembly, the test section is then compressed using spring-loaded bolts to ensure a consistent interfacial pressure between the heater and heat sink. All sensor measurements are collected at 0.5 Hz with a data acquisition system (Agilent, 34970A) utilizing a 20-channel multiplexer (Agilent, 34901A).

C. Test Procedure

Prior to conducting any tests, the heat loss is estimated by assembling the test section and applying power to the heater without any fluid present. The steady-state heat sink base temperature is recorded as a function of power input, allowing for correlation of the temperature-dependent heat loss during thermal testing based on the base temperature. A best-fit line through the heat loss calibration test data, assuming a zero intercept, yields an empirical correlation for the heat loss. Heat loss ranges from 1.4% to 3.2% for the heat inputs investigated in the current study. Prior to testing, fluid is allowed to flow through the heat sink for several minutes in order to flush out any loose particles that might be inside following fabrication; a bypass line is used during this flushing at flow rates beyond 500 mL/min.

To characterize the hydraulic performance, the flow rate through the unheated test section is incremented in steps of ~33 mL/min over a range from 100 mL/min to 500 mL/min. Steady flow conditions are achieved at each flow rate and the pressure drop across the test section is measured.

To characterize the thermal performance, the heater power is incremented from 0 W to 200 W in steps of 10 W at each fixed value of flow rate. The heat sinks were each tested at four flow rates of 120 mL/min, 241 mL/min, 361 mL/min, and 482 mL/min (corresponding to mass fluxes of 500 kg/m^{2}s, 1000 kg/m^{2}s, 1500 kg/m^{2}s, and 2000 kg/m^{2}s). At each test point, the system is allowed to reach steady-state conditions and then data are recorded for 60 s; the data are time-averaged over this period to give a single value for each measured variable at each test point. The flow is considered steady when the variation in pressure drop is less than 50 Pa and the temperature variation is less than 0.1 °C.

D. Data Reduction

The Reynolds number of the flow is calculated as

$$Re = \frac{GD_H}{\mu_l} \tag{1}$$

where the mass flux is calculated from the measured flow rate according to

$$G = \frac{\dot{V}\rho_l}{A_{ch}} \tag{2}$$

The Fanning friction factor of the heat sink is calculated directly from the pressure drop measured using the differential pressure transducer as

$$f_F = \frac{\rho_l \Delta P D_H}{2L_{ch}G^2} \tag{3}$$

For the straight microchannel design, the measured friction factor for developing flow in the laminar regime is compared to a value predicted based on correlations from the literature. The fully developed Fanning friction factor can be predicted by [39]

$$f_{F,fd} = \left(\frac{24}{Re}\right)(1 - 1.3553\alpha + 1.9467\alpha^2 - 1.7012\alpha^3 + 0.9564\alpha^4 - 0.2537\alpha^5) \tag{4}$$

The developing flow length ($L_{dev} = 0.05ReD_H$) is a significant fraction of the channel length for the range of flow rates tested for the straight microchannel heat sink design. An additional correction factor (Hagenbach factor) must be considered to account for developing flow effects, and is given by [40]

$$K_\infty = 0.6796 + 1.2197\alpha + 3.38089\alpha^2 - 9.5921\alpha^3 + 8.9089\alpha^4 - 2.29959\alpha^5 \tag{5}$$

The developing friction factor is then calculated as [40]

$$f_{F,dev} = \frac{K_\infty D_H}{4L_{dev}} + f_{F,fd} \tag{6}$$

The friction factor correlations described above consider neither the minor losses associated with contraction from the inlet header into the channels nor the expansion from the channels into the outlet header, which are included in the measured pressure drop data. Hence, the minor pressure losses are estimated and added to the predicted channel pressure drop to facilitate a direct comparison to the measured value (3).

These minor pressure losses are calculated as follows [41], with the areas A_1 and A_2 being the cross-sectional area, f_1 and f_2 the friction coefficients, D_1 and D_2 the hydraulic diameters, and L_1 and L_2 the lengths of the header and the channels, respectively.

$$\Delta P_{in} = (0.5\rho_l u_2^2)\left(1 - \left(\frac{A_2}{A_1}\right)^2 + 1.433 + \left(\frac{f_1 L_1}{D_1}\right) + \left(\frac{f_2 L_2}{D_2}\right)\right) \quad (7)$$

$$\Delta P_{out} = (0.5\rho_l u_2^2)\left(\left(\frac{A_2}{A_1}\right)^2 - 1 + \left(1 - \frac{A_2}{A_1}\right)^2 + \left(\frac{f_1 L_1}{D_1}\right)\right) \quad (8)$$

Due to the very large value of the relative roughness of the channel inner walls, for which turbulent flow friction factors correlations are not available, the measured data are not compared to predictions in the turbulent regime.

The thermal performance is characterized using the overall heat sink resistance, calculated directly from the measured base and fluid inlet temperatures and loss-adjusted heat input.

$$R_{tot} = \frac{T_{base} - T_{l,in}}{Q_{in}} \quad (9)$$

For the straight microchannel design, the overall resistance can be decomposed via a resistance network into four constituent parts representing the resistances due to conduction through the heat sink base, conduction through the channel walls, convective resistance between the channel walls and the heat transfer fluid, and caloric resistance within the fluid along the channel length, respectively given as:

$$R_{cond} = \frac{T_{base} - T_{wall,base}}{Q_{in}} = \frac{L_{base}}{k_s A_{ch}} \quad (10)$$

$$R_{wall} = \frac{T_{wall,base} - T_{wall,avg}}{Q_{in}} \quad (11)$$

$$R_{conv} = \frac{T_{wall,avg} - T_{f,avg}}{Q_{in}} = \frac{1}{hA_S} \quad (12)$$

$$R_{cal} = \frac{T_{l,avg} - T_{l,in}}{Q_{in}} \quad (13)$$

This decomposition of the total resistance allows a heat transfer coefficient to be extracted from the experiments. The caloric resistance is directly evaluated from measured values. The conduction and fin wall resistances are estimated as follows by assuming the thermal conductivity is equal to the nominal value for the material used (k_s = 110 W/m-K) [38]. The wall base temperature was calculated assuming one-dimensional conduction across the base thickness (10). The average wall temperature was calculated assuming that the wall acts like a fin with adiabatic tip conditions, using a corrected fin length of 1.5 times the channel height to account for four-sided conduction around the channel.

$$\eta_{fin} = \frac{\tanh(mL_{fin})}{mL_{fin}} \quad (14)$$

$$\eta_o = 1 - \frac{16A_{ch}}{A_{tot}}\left(1 - \eta_{fin}\right) \quad (15)$$

$$m = \sqrt{\frac{hP_{fin}}{k_s A_{fin}}} \quad (16)$$

This differs from prior experimental studies that assume three-sided conduction for cases where the top lid is a different, insulative material through which no heat is assumed to be transferred to the fluid. An iterative process is used to calculate the average fin wall temperature. An initial guess of unity is assumed for the overall surface efficiency to allow calculation of the heat transfer coefficient and individual fin efficiency; these values are then used to determine an adjusted surface efficiency. This iterative process continues until the initial and adjusted values converge to within 0.1%. The average fin temperature, and hence convective resistance, is then trivially calculated by knowing the converged heat transfer coefficient. The heat transfer coefficient is used to calculate the heat sink Nusselt number.

$$Nu = \frac{hD_H}{k_l} \quad (17)$$

The measured heat transfer performance within the laminar flow regime is compared to that predicted using correlations. An average Nusselt number over the channel length, weighted to account for the extent of the developing and fully developed portions of the flow, is calculated and compared to the measured data. The constant Nusselt number for fully developed laminar flow in rectangular channels is calculated using [42]

$$Nu_{fd} = 8.235\left(1 - \frac{1.883}{\alpha} + \frac{3.767}{\alpha^2} - \frac{5.814}{\alpha^3} + \frac{5.361}{\alpha^4} - \frac{2}{\alpha^5}\right) \quad (18)$$

The flow in the heat sink is simultaneously hydrodynamically and thermally developing; the average Nusselt number in that region is given as [43]

$$Nu_{dev} = 1.86\left(\frac{RePrD_H}{L}\right)^{\frac{1}{3}}\left(\frac{\mu_l}{\mu_{wall}}\right)^{0.14} \quad (19)$$

E. Uncertainty

The measurement uncertainties of the sensors used are listed in Table II, per the manufacturer specification sheets. The uncertainty in the calculated values was determined using the sequential perturbation method [44] and are also listed. The friction factor uncertainty is dependent on both the flow rate and differential pressure measurements, and is highest at low flow rates over the range of Reynolds numbers investigated. The thermal resistance and Nusselt number uncertainties are dominated by the uncertainty in the temperature measurements, which is highest at low powers where the temperature difference between the heat sink and fluid is low. Above inputs of 50 W, the relative uncertainty is under 10% for both R_{tot} and Nu.

IV. RESULTS

The hydraulic and thermal performance for the two heat sink designs is presented here. The performance of the straight microchannel (SMC) heat sink is compared to predicted values from commonly used laminar-flow correlations in order to determine how the behavior of additively manufactured heat sinks may differ from conventional theory, due to their method of fabrication. Results for the manifold microchannel (MMC) heat sink demonstrate the ease of fabrication of complex structures via additive manufacturing in order to achieve a pressure drop reduction.

A. Hydraulic Results

Fig. 5 shows the measured Fanning friction factor (3) as a function of the Reynolds number for the straight microchannel heat sink. The trend in friction factor matches the conventional behavior for internal flow: there is a monotonic decrease with increasing Reynolds number in the laminar regime, followed by transition to a higher, relatively constant value for turbulent flow. The transition occurs at a critical Re of ~600, based on the location of the minimum friction factor. Although this transition occurs at a relatively low Reynolds number compared to smooth channels, the value lies within the expected range for

very rough microchannels, in which transition has been observed to occur at Reynolds numbers as low as 500 [45], [46]. Assuming the internal roughness of the 500 μm channels is as large as that measured for the outer surfaces (Ra = 20 μm), early transition should be expected for this high relative roughness of ~4%. Because microchannel heat sinks are often designed assuming laminar flow behavior, this early transition to turbulence is an important factor when considering the design and use of additively manufactured heat sinks.

The measured friction factor is compared to laminar-flow predictions for the straight microchannel design in Fig. 5. The friction factor behavior is reasonably predicted in the laminar regime; the corresponding pressure drop predictions are accurate to within ±0.5 kPa prior to the critical Reynolds number, beyond which the measurements diverge from laminar theory as the flow transitions to turbulence. Though the roughness introduced by the fabrication process causes early transition to turbulence, the hydraulic behavior of the straight microchannel heat sink is predictable with conventional theory within the laminar regime. This indicates that the target dimensions of the heat sinks were achieved in the fabrication process and confirms that heat sinks can be additively manufactured with features sizes as small as 500 μm while still meeting predicted hydraulic performance targets.

Fig. 6 compares the measured pressure drops across the straight microchannel and manifold microchannel heat sink designs over the same range of Reynolds numbers. The MMC design yields a lower pressure drop across the range of Reynolds numbers tested. At the lowest flow rates, the reduction can be as large as 90% (Re = 210); at higher flow rates, the reduction in pressure drop is approximately 40% (Re = 1175). From inspecting the location of the change in slope of the pressure drop curves, it appears that the manifold design also demonstrates an early transition to turbulence at Re = ~800. The roughness inherent to DMLS fabrication is found to restrict the range of the laminar design space. Nevertheless, this result demonstrates successful design and additive manufacture of more complex heat sink features that are capable of reducing pressure drop.

B. Thermal Results

For a given heat sink geometry and flow rate, the thermal resistance is expected to be constant with power input during single-phase operation; changes in heat flux translate to proportional changes in the streamwise temperature gradient within the fluid and the local temperature difference between the convection surface and the bulk fluid. Per the test methodology (Section III.C), data were collected across a range of power inputs from 0 to 200 W. The values of thermal resistance across the entire range of power are all within 7% of the reported mean values at each flow rate (see Appendix). Due to the near-constant values across each range of power inputs, the following discussion refers to the arithmetic mean of all test points for a given heat sink and flow rate.

The measured total thermal resistance is decomposed into the component resistances specified in (10)-(13). Across the four flow rates tested, the convective resistance contributed between 71.5-75.5% of the total thermal resistance, indicating that heat sink performance was not primarily governed by conduction through the solid geometry; fin efficiencies were calculated to be in the range of 0.93 to 0.97. The measured Nusselt number of the straight microchannel design is shown in Fig. 7 at each flow rate. Because of the developing flow conditions in the heat sink, the Nusselt number increases with Reynolds number; higher heat transfer is achieved at the higher flow rates. The three highest mass flux cases are not in a laminar regime, but have relatively low Reynolds numbers (661, 974, and 1298) for which turbulent heat transfer correlations are not valid; this presents a challenge for predicting the performance of the additively manufactured heat sinks in the present study that undergo early transition to turbulence.

The Nusselt number can be predicted and compared to the measured value for the lowest Reynolds number case that lies in the laminar flow regime. The predicted laminar Nusselt number accounting for developing flow effects is 45% higher than the measured value (5.93 versus 4.08). Whereas the successful hydraulic performance comparison suggested that the nominal microchannel geometry was adequately reproduced (Section IV.A), this thermal performance comparison raises the question of whether the material thermal properties (*viz.*, thermal conductivity) and base/fin resistances can be adequately approximated using the nominal thermal conductivity values of printed material [38]; for example, an under-estimate of these conduction resistances while extracting the Nusselt number from the experimental data would lead to this observed overprediction. Further investigation is required to identify the cause for the mismatch in the thermal performance between the measured and predicted values. Along with surface roughness, the uncertainty in the properties of additively manufactured materials poses a challenge to predictive design of AM microchannel heat sinks.

The overall thermal resistances of the straight microchannel and manifold microchannel heat sink designs are compared as a function of Reynolds number in Fig. 8. The MMC designs display the same decreasing trend in resistance with increasing Reynolds number as was previously discussed for the SMC design. However, the MMC design has a higher thermal resistance across the range of mass flux tested, ranging from 0.65 K/W to 0.45 K/W compared to a range from 0.50 K/W and 0.29 K/W for the SMC design.

The primary function of the added geometric complexity of the manifold design is to reduce the maximum flow length along each flow path in the microchannel; this goal was successfully achieved in terms of the reduced pressure drop (Fig. 6). However, both microchannel heat sink designs utilize the same-sized square microchannel geometry, which would be expected to yield similar heat transfer performance, aside from developing flow effects. While manifold microchannel heat sink designs can potentially offer improved thermal performance due to an increase in the percentage of developing flow along the shorter channel length [8], this trend is not observed in the current data (Fig. 8). We speculate that this is due to the difference in convective area between the two designs; the SMC heat sink has all four sides of the channel available for convection, whereas the MMC heat sink has only three, with the manifold on the fourth side. This is an important example of how the perceived benefits of additively manufacturing a heat sink (monolithic, no layer-bonding) may have such unexpected drawbacks that must be anticipated at the design stage. This calls for revision of notional heat sink design

guidelines accounting for such factors to accommodate additive manufacturing techniques. Additionally, future work should target narrower channels of higher aspect ratio (depth to width), for which the use of a manifold design is known to improve the thermal performance at an equivalent pressure drop compared to straight microchannel designs [8]. This would better justify the added geometric complexity enabled by additive manufacturing.

The insights gained from this study, which offers an improved description of the fabrication constraints and sets expectations on fidelity to the design targets, will be used in ongoing work that explores heat sink designs exploiting features unique to additive manufacturing. The geometric freedom and complexity allowed by this technology has the potential to usher in a new generation of designs that benefit from nearly unrestricted optimization and shapes beyond those that can be currently produced, while also being smaller and lighter. It also has relevance beyond microchannels and could expand into other areas of thermal management and larger-scale heat exchangers, ultimately allowing for one-off, application- and performance-specific solutions.

V. Conclusions

The current study designed and experimentally characterized additively manufactured microchannel heat sinks targeted for electronics cooling applications. A straight microchannel (SMC) heat sink and a manifold microchannel (MMC) heat sink were designed, representative of simple and intermediate geometric complexities. The SMC design allows direct comparison of the hydraulic and thermal performance against predictive models to assess part fidelity; the MMC design allows demonstration of monolithic integration of flow manifolds via additive manufacturing. Both designs were fabricated in an aluminum alloy using a commercial DMLS machine following a survey of additive manufacturing technologies; downselection was based on features desirable for this particular microchannel heat sink application. The conclusions of this survey can be translated to other thermal management applications based on the specific feature requirements. The fabricated heat sinks had high surface roughness, above the quoted range of the material and process. Material porosity was measured to be less than 0.1% utilizing non-destructive micro-CT scanning.

Both the SMC and MMC heat sinks were experimentally tested in single-phase operation over a range of flow rates and heat inputs, using water as the working fluid. The results show that the hydraulic performance of the SMC heat sink is well-predicted by established correlations when the flow is laminar. The high internal roughness leads to an early transition to turbulence ($Re < 800$) for both heat sinks, limiting the range of operation predictable using standard correlations for laminar flow. The incorporation of a manifold reduced the pressure drop by 40-90% across the range of flow rates tested, without incurring any significant fabrication effort beyond that of the straight microchannel design. A mismatch between the measured and predicted thermal performance for the SMC heat sink suggests that the nominal material thermal properties might not yield accurate estimates of the conduction resistances in the heat sink. The present work expands on the limited research into additive manufacturing of microchannel heat sinks, demonstrating the applicability of conventional hydrodynamic theory to samples produced by additive manufacturing, while also highlighting several challenges associated with design in this new manufacturing domain.

Appendix

The total thermal resistance (9) is shown as a function of power input for the straight and manifold microchannel designs in Figs. A1 and A2, respectively. These plots illustrate the individual test points that have been averaged for each flow rate for presentation in Section IV, as well as the variation of uncertainty with power.

Acknowledgment

Special thanks to Dr. James C. Williams Jr. (Indiana University School of Medicine) for performing the μCT scanning of samples and to Serdar Ozguc (Purdue University) for discussion of the results and data processing.

References

[1] G. L. Morini, “Single-phase convective heat transfer in microchannels: a review of experimental results,” *Int. J. Therm. Sci.*, vol. 43, no. 7, pp. 631–651, 2004.

[2] S. V. Garimella and C. B. Sobhan, “Transport in microchannels - a critical review,” *Annu. Rev. Heat Transf.*, vol. 13, no. 13, pp. 1–50, 2003.

[3] H. H. Bau, “Optimization of conduits’ shape in micro heat exchangers,” *Int. J. Heat Mass Transf.*, vol. 41, no. 18, pp. 2717–2723, 1998.

[4] J. Li and G. P. Peterson, “3-Dimensional numerical optimization of silicon-based high performance parallel microchannel heat sink with liquid flow,” *Int. J. Heat Mass Transf.*, vol. 50, no. 15, pp. 2895–2904, 2007.

[5] P. Gunnasegaran, H. A. Mohammed, N. H. Shuaib, and R. Saidur, “The effect of geometrical parameters on heat transfer characteristics of microchannels heat sink with different shapes,” *Int. Commun. Heat Mass Transf.*, vol. 37, no. 8, pp. 1078–1086, 2010.

[6] G. M. Harpole and J. E. Eninger, “Micro-channel heat exchanger optimization,” in *Proc. 7th IEEE Semiconductor Thermal Measurement Manage. Symp. (SEMI-THERM)*, 1991, pp. 59–63.

[7] N. Tran, Y.-J. Chang, J. Teng, T. Dang, and R. Greif, “Enhancement thermodynamic performance of microchannel heat sink by using a novel multi-nozzle structure,” *Int. J. Heat Mass Transf.*, vol. 101, pp. 656–666, 2016.

[8] J. H. Ryu, D. H. Choi, and S. J. Kim, “Three-dimensional numerical optimization of a manifold microchannel heat sink,” *Int. J. Heat Mass Transf.*, vol. 46, no. 9, pp. 1553–1562, 2003.

[9] S. Sarangi, K. K. Bodla, S. V. Garimella, and J. Y. Murthy, “Manifold microchannel heat sink design using optimization under uncertainty,” *Int. J. Heat Mass Transf.*, vol. 69, pp. 92–105, 2014.

[10] R. Mandel, S. Dessiatoun, P. McCluskey, and M. Ohadi, “Embedded Two-Phase Cooling of High Flux Electronics via Micro-Enabled Surfaces and Fluid Delivery Systems (FEEDS),” in *International Technical Conference and Exhibition on Packaging and Integration of Electronic and Photonic Microsystems (InterPACK) and International Conference on Nanochannels, Microchannels and Minichannels (ICNMM)*, 2015, p. V003T10A012.

[11] K. P. Drummond, D. Back, M. D. Sinanis, D. B. Janes, D. Peroulis, J. A. Weibel, and S. V. Garimella, “Characterization of hierarchical manifold microchannel heat sink arrays under simultaneous background and hotspot heating conditions,” *Int. J. Heat Mass Transf.*, (in review).

[12] H. Kodama, “Automatic method for fabricating a three-dimensional plastic model with photo-hardening polymer,” *Rev. Sci. Instrum.*, vol. 52, no. 11, pp. 1770–1773, 1981.

[13] T. Wohlers and T. Gornet, “History of additive manufacturing,” Wohlers Associates, Inc., Fort Collins, CO, USA, 2014.

[14] C. R. Deckard, "Method and apparatus for producing parts by selective sintering," U.S. Patent 4863538 A, Sept. 5, 1989.
[15] R. Liu, Z. Wang, T. Sparks, F. Liou, and J. Newkirk, "Aerospace applications of laser additive manufacturing," in *Laser Additive Manufacturing*, Elsevier, 2017, pp. 351–371.
[16] P. R. Gradl, C. Protz, S. E. Greene, D. Ellis, B. Lerch, and I. Locci, "Development and hot-fire testing of additively manufactured copper combustion chambers for liquid rocket engine applications," NASA, Huntsville, AL, USA, Rep. M17-6434, 2017.
[17] P. Gradl, S. E. Greene, C. Protz, D. Ellis, B. Lerch, and I. Locci, "Additive manufacturing overview: propulsion applications, design for and lessons learned," in *53rd AIAA/SAE/ASEE Joint Prop. Conf., AIAA Prop. Energy Forum*, 2017, p. AIAA 2017-4670.
[18] A. Uriondo, M. Esperon-Miguez, and S. Perinpanayagam, "The present and future of additive manufacturing in the aerospace sector: A review of important aspects," *Proc. Inst. Mech. Eng. Part G J. Aerosp. Eng.*, vol. 229, no. 11, pp. 2132–2147, 2015.
[19] C. K. Stimpson, J. C. Snyder, K. A. Thole, and D. Mongillo, "Roughness effects on flow and heat transfer for additively manufactured channels," *J. Turbomach.*, vol. 138, no. 5, p. 051008, 2016.
[20] C. K. Stimpson, J. C. Snyder, K. A. Thole, and D. Mongillo, "Scaling roughness effects on pressure loss and heat transfer of additively manufactured channels," *J. Turbomach.*, vol. 139, no. 2, p. 021003, 2016.
[21] J. C. Snyder, C. K. Stimpson, K. A. Thole, and D. Mongillo, "Build direction effects on additively manufactured channels," *J. Turbomach.*, vol. 138, no. 5, p. 051006, 2016.
[22] K. L. Kirsch and K. A. Thole, "Pressure loss and heat transfer performance for additively and conventionally manufactured pin fin arrays," *Int. J. Heat Mass Transf.*, vol. 108, pp. 2502–2513, 2017.
[23] K. L. Kirsch, J. C. Snyder, C. K. Stimpson, K. A. Thole, and D. Mongillo, "Repeatability in performance of micro cooling geometries manufactured with laser powder bed fusion," in *AIAA Propulsion and Energy Forum*, 2017, p. AIAA 2017-4706.
[24] M. A. Arie, A. H. Shooshtari, V. V. Rao, S. V. Dessiatoun, and M. M. Ohadi, "Air-side heat transfer enhancement utilizing design optimization and an additive manufacturing technique," *J. Heat Transf.*, vol. 139, no. 3, p. 031901, 2017.
[25] M. A. Arie, A. H. Shooshtari, S. V. Dessiatoun, and M. M. Ohadi, "Performance characterization of an additively manufactured titanium (Ti64) heat exchanger for an air-water cooling application," in *ASME Summer Heat Transfer Conference (SHTC) collocated with the ASME Fluids Engineering Division Summer Meeting and the ASME International Conference on Nanochannels, Microchannels, and Minichannels (ICNMM)*, 2016, p. V002T22A002.
[26] D. M. Hymas, M. A. Arle, F. Singer, A. H. Shooshtari, and M. M. Ohadi, "Enhanced air-side heat transfer in an additively manufactured polymer composite heat exchanger," in *IEEE Intersociety Conference on Thermal and Thermomechanical Phenomena in Electronic Systems (ITherm)*, 2017, pp. 634–638.
[27] E. M. Dede, S. N. Joshi, and F. Zhou, "Topology optimization, additive layer manufacturing, and experimental testing of an air-cooled heat sink," *J. Mech. Des.*, vol. 137, no. 11, p. 111403, 2015.
[28] M. Wong, S. Tsopanos, C. J. Sutcliffe, and I. Owen, "Selective laser melting of heat transfer devices," *Rapid Prototyp. J.*, vol. 13, no. 5, pp. 291–297, 2007.
[29] W. D. Gerstler and D. Erno, "Introduction of an additively manufactured multi-furcating heat exchanger," in *IEEE Intersociety Conference on Thermal and Thermomechanical Phenomena in Electronic Systems (ITherm)*, 2017, pp. 624–633.
[30] U. Scheithauer, E. Schwarzer, T. Moritz, and A. Michaelis, "Additive manufacturing of ceramic heat exchanger: opportunities and limits of the lithography-based ceramic manufacturing (lcm)," *J. Mater. Eng. Perform.*, vol. 27, no. 1, pp. 14–20, 2018.
[31] F. Calignano, D. Manfredi, E. P. Ambrosio, L. Iuliano, and P. Fino, "Influence of process parameters on surface roughness of aluminum parts produced by DMLS," *Int. J. Adv. Manuf. Technol.*, vol. 67, no. 9–12, pp. 2743–2751, 2013.
[32] H. Bikas, P. Stavropoulos, and G. Chryssolouris, "Additive manufacturing methods and modelling approaches: a critical review," *Int. J. Adv. Manuf. Technol.*, vol. 83, no. 1–4, pp. 389–405, 2016.
[33] W. E. Frazier, "Metal additive manufacturing: a review," *J. Mater. Eng. Perform.*, vol. 23, no. 6, pp. 1917–1928, 2014.
[34] I. Gibson, D. Rosen, and B. Stucker, *Additive Manufacturing Technologies*. New York, NY: Springer New York, 2015.
[35] M. Vaezi, H. Seitz, and S. Yang, "A review on 3D micro-additive manufacturing technologies," *Int. J. Adv. Manuf. Technol.*, vol. 67, no. 5–8, pp. 1721–1754, 2013.
[36] C. Atwood, M. Ensz, D. Greene, M. Griffith, L. Harwell, D. Reckaway, T. Romero, E. Schlienger, and J. Smugeresky, "Laser engineered net shaping (LENS): a tool for direct fabrication of metal parts," Sandia National Laboratories, Albuquerque, NM, and, Livermore, CA, SAND98–2473C, 1998.
[37] Y. Bai and C. B. Williams, "An exploration of binder jetting of copper," *Rapid Prototyp. J.*, vol. 21, no. 2, pp. 177–185, Mar. 2015.
[38] Electro Optical Systems GmbH, "Material Data Sheet - EOS Aluminum AlSi10Mg" datasheet, May 2014.
[39] R. K. Shah and A. L. London, *Laminar Flow Forced Convection In Ducts*. NY, USA: Academic Press, 1978.
[40] M. E. Steinke and S. G. Kandlikar, "Single-phase liquid friction factors in microchannels," *Int. J. Therm. Sci.*, vol. 45, no. 11, pp. 1073–1083, 2006.
[41] R. Blevins, *Applied Fluid Dynamics Handbook*. NY, USA: Van Nostrand Reinhold Co., 1984.
[42] W. Kays and M. Crawford, *Convective Heat and Mass Transfer*, 2nd ed. NY, USA: McGraw-Hill, 1980.
[43] E. N. Sieder and G. E. Tate, "Heat transfer and pressure drop of liquids in tubes," *Ind. Eng. Chem.*, vol. 28, no. 12, pp. 1429–1435, 1936.
[44] R. J. Moffat, "Using uncertainty analysis in the planning of an experiment," *J. Fluids Eng.*, vol. 107, no. 2, pp. 173–178, 1985.
[45] X. F. Peng and G. P. Peterson, "Convective heat transfer and flow friction for water flow in microchannel structures," *Int. J. Heat Mass Transf.*, vol. 39, no. 12, pp. 2599–2608, 1996.
[46] G. M. Mala and D. Li, "Flow characteristics of water in microtubes," *Int. J. Heat Fluid Flow*, vol. 20, no. 2, pp. 142–148, 1999.

Ivel L. Collins received the B.S. degree in mechanical engineering from the Rose-Hulman Institute of Technology in 2016. He is currently pursuing the M.S. degree in the School of Mechanical Engineering from Purdue University as a research assistant in the Cooling Technologies Research Center, where his work focuses on the intersection of additive manufacturing and high-performance electronics cooling.

Ivel Collins is a recipient of the Helen and John Lozar Assistantship.

Justin A. Weibel is a Research Associate Professor in the School of Mechanical Engineering at Purdue University and serves as the Associate Director of the Cooling Technologies Research Center (CTRC). He received his PhD in 2012 and BSME in 2007, both from Purdue University. Dr. Weibel's research explores methodologies for prediction and control of phase-change and heat transport across interfaces to enhance the performance and efficiency of thermal management technologies, energy transfer processes, and other multiphase and psychrometric thermal systems. Projects span across fluid-thermal transport, surface and interfacial science, and microfabrication disciplines. He received the 2011 ASME Electronic & Photonic Packaging Division (EPPD) Student Member of the Year Award.

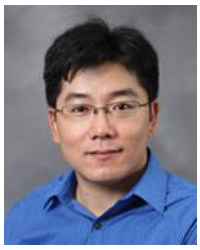

Liang Pan is an Assistant Professor of Mechanical Engineering and Birck Nanotechnology Center at Purdue University, West Lafayette, IN, USA. He received his M.S. and Ph.D. in Mechanical Engineering from UC Berkeley in 2009 and 2010, and B.S. and M.E. from University of Science and Technology of China.

Prior joining Purdue, he worked as a Postdoctoral Researcher in the NSF's Nano-scale Science and Engineering Center (NSEC) for Scalable and Integrated Nanomanufacturing (SINAM). Dr. Pan studies light-matter interactions with an emphasis on developing novel micro- and nano-manufacturing processes, products and systems for lithography, data storage, communication, and thermal and energy applications.

Dr. Pan was a recipient of the 2016 NSF CAREER Award.

Suresh V. Garimella is Executive Vice President for Research and Partnerships and the Goodson Distinguished Professor of Mechanical Engineering at Purdue University, West Lafayette, IN, USA, where he is also the Director of the National Science Foundation Cooling Technologies Research Center. He has supervised over 90 Ph.D. and M.S. students, has co-authored 525 refereed journal and conference publications, and holds 13 patents. Twenty-four alumni from his research group are now faculty members at prestigious universities around the world. His research group has made seminal contributions to micro and nanoscale thermal and fluidic engineering, novel materials for thermal management, materials processing and manufacturing, and renewable energy.

Dr. Garimella serves as editor with several leading journals. He is a Fellow of the National Academy of Inventors, and of AAAS and ASME. His contributions to thermal management were recognized with the 2016 ITHERM Achievement Award.

Table I. Comparison of AM process capabilities suitable for microchannel heat sink applications based on commericial vendor specifications.

Process	**Minimum Feature Size**	**Tolerance**	**Commonly Available Materials**	**Cost**
DMLS	150 - 400 µm	50 - 250 µm	Tool steels, Stainless Steel, AlSi10Mg, Inconel, Ti64, Tungsten, Molybdenum	$
EBM	150 - 400 µm	50 - 250 µm	Tool steels, Stainless Steel, AlSi10Mg, Inconel, Ti64	$
EFAB	4 - 25 µm	2 µm	Nickel-cobalt, palladium, rhodium, copper alloys	$$$

Table II. Uncertainty in measured and calculated values.

Measured Value	**Uncertainty**
Pressure drop	± 0.172 kPa
Volumetric flow rate	± 5 mL/min
Temperature	± 1.0 °C
Voltage	± < 1%
Calculated Value	**Mean Uncertainty (Range)**
f_F	14.1% (2% - 21%)
R_{tot}	6.9% (1.5% - 50%)
Nu	10.7% (1.7% - 54%)

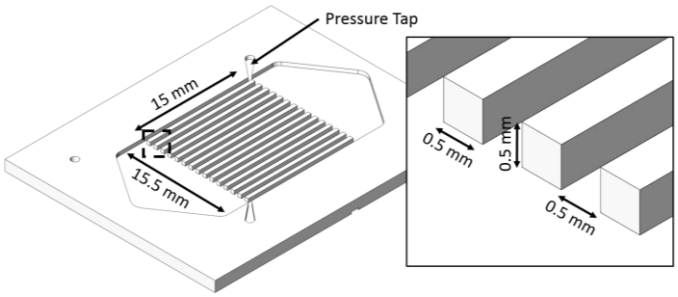

(a)

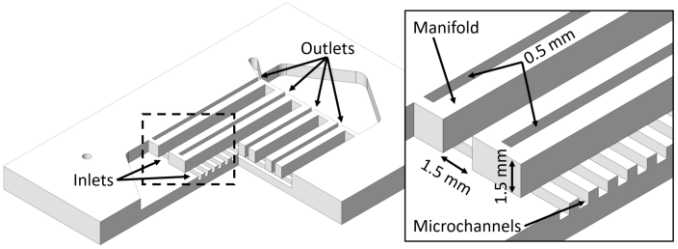

(b)

Figure 1. Geometries of the (a) straight microchannel (SMC) and (b) manifold microchannel (MMC) heat sink designs.

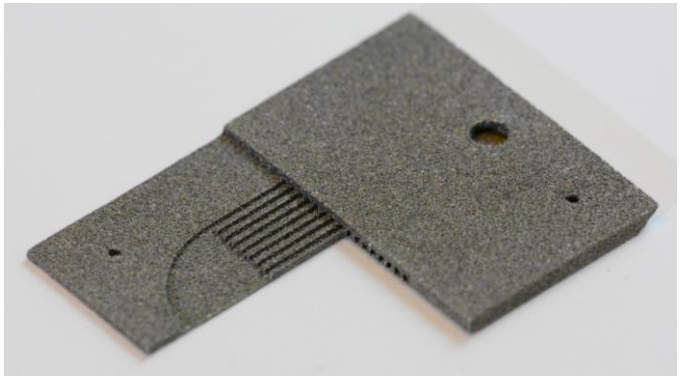

(a)

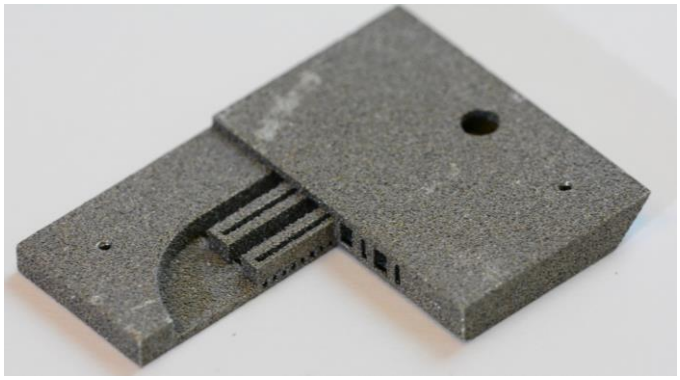

(b)

Figure 2. Images of the (a) SMC and (b) MMC additively manufactured heat sinks. These samples were produced with sections removed to allow for visualization of the channel geometry.

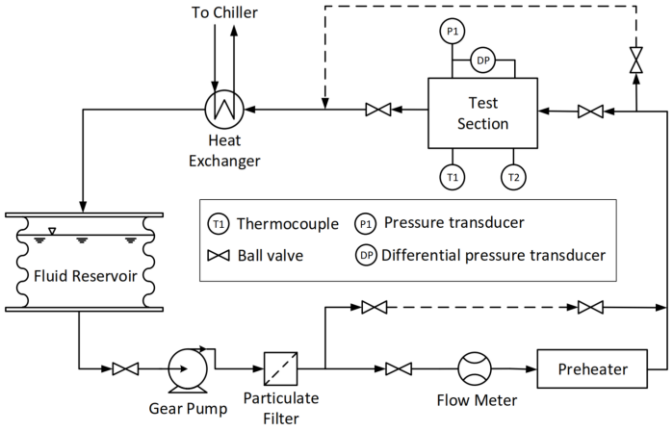

Figure 3. Schematic diagram of the experimental flow loop facility.

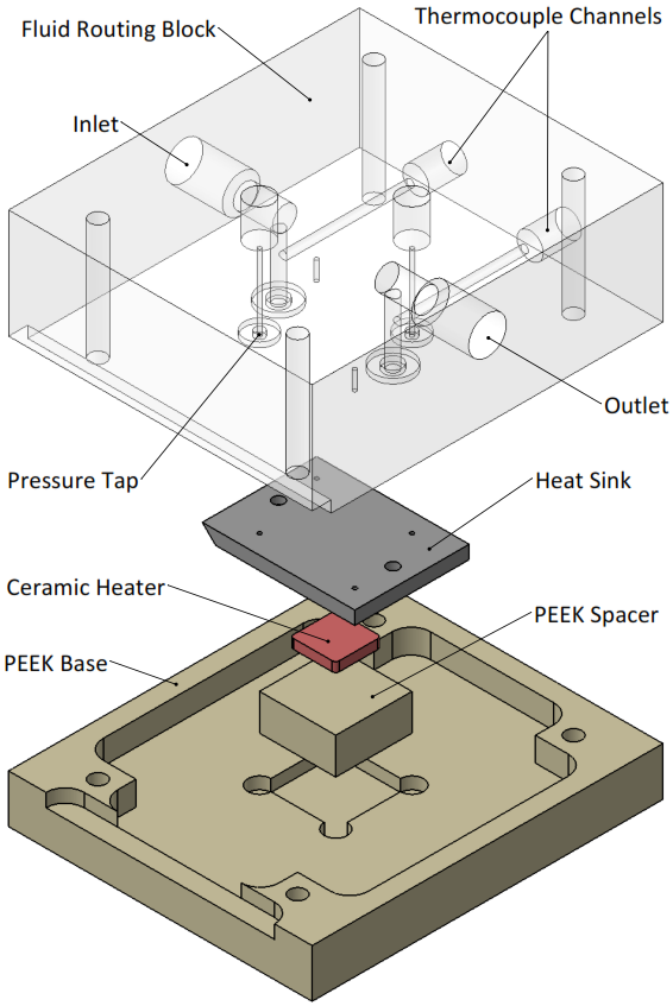

Figure 4. Exploded model of the test section. The fluid fittings, thermal pad, and bolts are not shown.

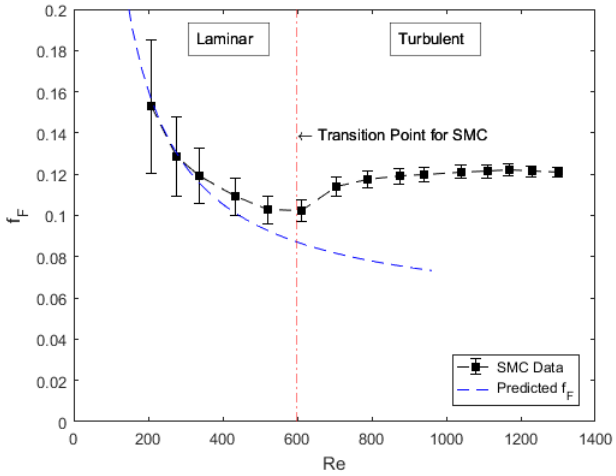

Figure 5. Fanning friction factor variation as a function of Reynolds number for the straight microchannel (SMC) heat sink. The dashed vertical line marks the start of transition from laminar to turbulent behavior.

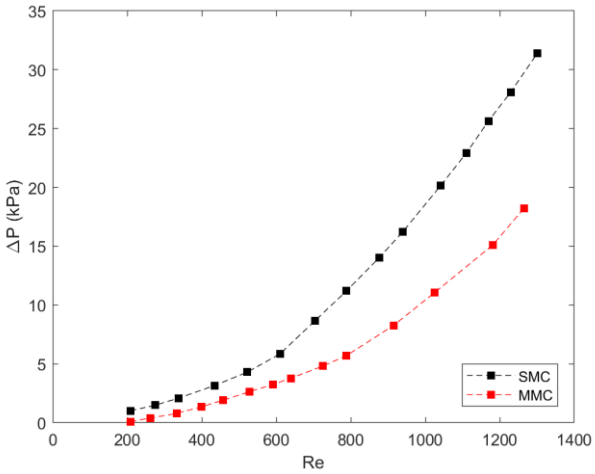

Figure 6. Comparison of measured straight microchannel (SMC) and manifold microchannel (MMC) heat sink pressure drop as a function Reynolds number (± 0.172 kPa error bars not shown).

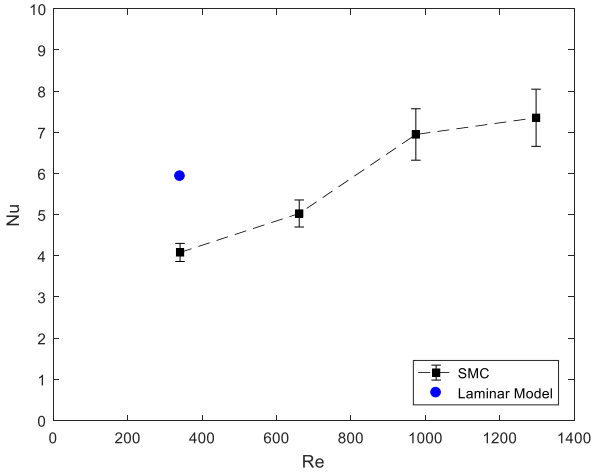

Figure 7. Measured Nusselt number as a function of Reynolds number for the straight microchannel (SMC) design. A predicted Nusselt number is shown at a single Reynolds number in the laminar regime.

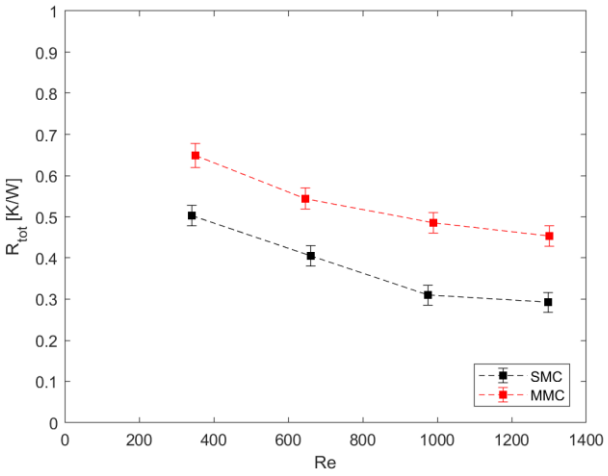

Figure 8. Comparison of thermal resistance variation with Reynolds number for the two additively manufactured heat sink designs.

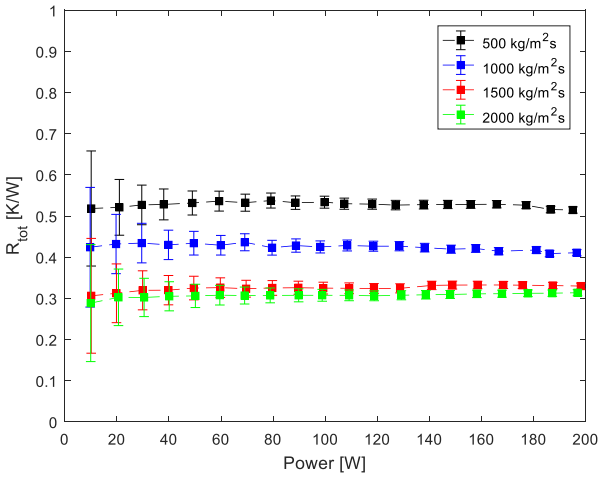

Figure A1. Measured total thermal resistance as a function of power input for the straight microchannel (SMC) design.

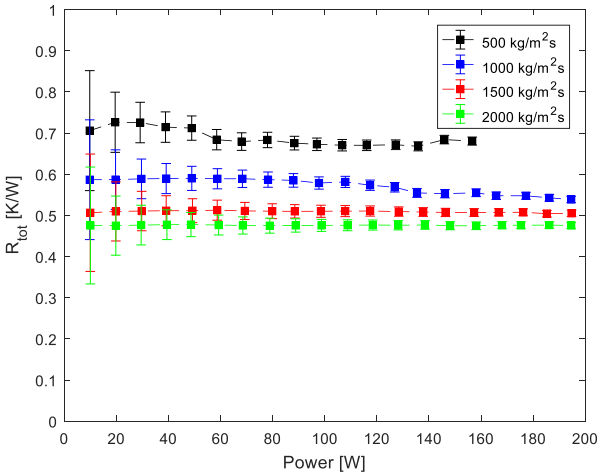

Figure A2. Measured total thermal resistance as a function of power input for the manifold microchannel (MMC) design.